THE ASTROPHYSICAL JOURNAL, 494:111–117, 1998 February 10


# K-BAND GALAXY COUNTS IN THE SOUTH GALACTIC POLE REGION

TAKEO MINEZAKI[1,2,3] AND YUKIYASU KOBAYASHI[1]
National Astronomical Observatory, Mitaka-shi, Tokyo 181, Japan;
minezaki@asterope.mtk.nao.ac.jp; yuki@merope.mtk.nao.ac.jp

YUZURU YOSHII[1,4]
Institute of Astronomy, Faculty of Science, University of Tokyo, Mitaka-shi, Tokyo 181, Japan;
yoshii@omega.mtk.ioa.s.u-tokyo.ac.jp

AND

BRUCE A. PETERSON
Mt. Stromlo and Siding Spring Observatories, Institute of Advanced Studies, The Australian National University,
Private Bag, Weston Creek, A.C.T. 2611, Australia; peterson@mso.anu.edu.au
*Received 1997 May 13; accepted 1997 September 16*

## ABSTRACT

We present new $K$-band galaxy number counts from $K = 13$ to 20.5 obtained from $K'$-band surveys in the south galactic pole region, which cover 180.8 arcmin$^2$ to a limiting magnitude of $K = 19$ and 2.21 arcmin$^2$ to $K = 21$. These are currently the most precise $K$-band galaxy counts at $17.5 < K < 19.0$ because the area of coverage is largest among the existing surveys for this magnitude range. The completeness and photometry corrections are estimated from the recovery of simulated galaxy and stellar profiles added to the obtained field image. Many simulations were carried out to construct a probability matrix that corrects the galaxy counts at the faint-end magnitudes of the surveys so the corrected counts can be compared with other observations. The $K$-band star counts in the south galactic pole region to $K = 17.25$ are also presented for use to constrain the vertical structure of the Galaxy.

*Subject headings:* cosmology: observations — galaxies: evolution — galaxies: photometry — galaxies: statistics — Galaxy: structure — infrared: galaxies — surveys

## 1. INTRODUCTION

A near-infrared survey of galaxies is fundamental for the study of cosmology. Merits of using the near-infrared wavelengths are that the $K$-corrections of galaxies remain small and nearly independent of their morphological type up to $z \sim 2$ (Cowie et al. 1994; Yoshii & Peterson 1995) and that the evolutionary corrections of galaxies are smooth and modeled reliably. This is because the luminosity of galaxies in the near-infrared is dominated by low-mass, late-type stars and is less sensitive to bursts of star formation (Yoshii & Takahara 1988), and even at large redshift, near-infrared observations of galaxies measure their flux in well-known optical wavelengths. Furthermore, the dust extinction in the near-infrared is much smaller than in the optical.

The $K$-band galaxy number counts have been obtained by a number of authors to a variety of depths in different areas in order to constrain the geometry of the universe (Gardner, Cowie, & Wainscoat 1993; Cowie et al. 1994; Gardner et al. 1995a, 1995b; Glazebrook et al. 1994; McLeod et al. 1995). Recently, Djorgovski et al. (1995) and Moustakas et al. (1997) surveyed small areas of a few square arcminutes to an extremely faint magnitude of $K \approx 23$ using the Keck telescope, while Gardner et al. (1996) and Huang et al. (1997) surveyed very large areas of about 10 deg$^2$ and presented very precise galaxy counts to $K \approx 16$.

In this paper, we present new results of $K$-band galaxy counts obtained from two surveys in the south galactic pole (SGP) region. The bright survey covers 180.8 arcmin$^2$ to the limiting magnitude of $K = 19$, and the faint survey covers 2.21 arcmin$^2$ to $K = 21$. The observations are described in § 2, and the image reduction procedures of flat fielding, image registration, and flux calibration are described in § 3. The detection and photometry of objects, star-galaxy separation, and star counts are described in § 4. The procedure of correcting the galaxy counts at faint-end magnitudes is described in § 5. The results of $K$-band galaxy counts are presented and discussed in § 6. Their cosmological interpretations will be presented in another paper.

## 2. OBSERVATIONS

The bright and faint surveys were carried out during 1994 August and September using the Australian National University's 2.3 m telescope at Siding Spring Observatory, Australia, equipped with the PICNIC near-infrared camera (Kobayashi et al. 1994), which was developed at National Astronomical Observatory, Japan. PICNIC uses a NICMOS3 array (256 × 256 pixels) with a field of view of 2.2 × 2.2 arcmin$^2$ and with a pixel scale of 0.″509 pixel$^{-1}$. In order to reduce the thermal sky background, we used a $K'$ filter, which has the same transmission curve as the 2MASS $K_S$ filter (McLeod et al. 1995).

The bright survey was centered at $(\alpha, \delta) = (0^h50^m48^s, -27°43'34'')$ (2000) or $(l, b) = (316.°27, -89.°39)$. The observations were made by raster scanning with the telescope. Each scan consisted of eight steps with 100″ offsets (30″ overlap) in right ascension followed by a step with the same 100″ offsets in declination and eight more steps in right ascension in the reverse direction until all 64 positions of an 8 × 8 grid had been observed by taking a set of expo-

[1] Visiting Astronomer, Siding Spring Observatory operated by The Australian National University.
[2] Department of Astronomy, School of Science, The University of Tokyo, Bunkyo-ku, Tokyo 113, Japan.
[3] Current address: Kiso Observatory, Institute of Astronomy, Faculty of Science, The University of Tokyo, Mitake-mura, Kiso-gun, Nagano 397-01, Japan; minezaki@kiso.ioa.s.u-tokyo.ac.jp.
[4] Research Center for the Early Universe, School of Science, The University of Tokyo, Bunkyo-ku, Tokyo 113, Japan.

sures at each grid position in the scan. Some scans took eight 17.1 s exposures at each grid position, others took five, depending on the time available to complete the observations. The scan pattern was observed seven times to obtain 58 exposures, i.e., 990 s integration per position.

The faint survey was centered at $(\alpha, \delta) = (0^h50^m54^s, -27°46'42'')$ (2000) or $(l, b) = (313.°35, -89.°34)$, within the area of the bright survey. The telescope was shifted randomly in such a pattern that no positions were closer than 3″ to each other and the positions cover a $30 \times 30$ arcsec$^2$ box. The integration time of each exposure was also 17.1 s, and eight exposures were taken at each position. The pattern was observed several times so that 2351 exposures were obtained, corresponding to a total integration time of 40,000 s.

## 3. REDUCTION

The images were reduced using IRAF[5] and STSDAS[6]. The raw $K'$-band images were corrected for thermal scattered light by subtracting a sky image and corrected for spatial variations in the detector response by dividing with a flat-field image after subtracting the sky image. A further correction was applied to remove residual thermal stray light and residual sky background variations.

The construction of the sky images, the flat-field images, and the mosaic required two iterations. The objects detected in the mosaicked image constructed for the first iteration were masked during the construction of the sky images and flat-field images for the second and final iteration.

The observations for the faint survey and bright survey were made in slightly different manners, and this necessitated slightly different treatments in the reductions. The faint survey observations were made by taking a series of sequential exposures with the telescope pointing at essentially the same position in the sky, with only small offsets made between every set of eight 17.1 s exposures. The faint survey field contained two stars that appeared in each exposure and were used to register all of the individual faint survey images.

The bright survey observations were made by raster scanning with the telescope. Each scan consisted of different 64 positions in an $8 \times 8$ grid. Eight or five in some scans 17.1 s exposures were taken at each grid position. The exposures at each grid position from a single scan were median combined to create a position image. If the individual exposures contained bright objects, then offsets between the different exposures at the same grid position were determined from the bright objects and used to construct the position image at that grid position. A scan image was constructed by median combining the 64 position images of each scan after registering them against an Anglo-Australian Telescope $I$-band CCD image in the first iteration and against the first iteration $K'$-band mosaicked image in the final iteration. In a few cases, a position image contained no objects suitable for registration, and the relative position in the scan was interpolated from the registered position images that preceded and followed in the scan sequence. The mosaicked image of the bright survey area was constructed by median combining the seven scan images after smoothing a few of the scans obtained in better seeing to the characteristic seeing of the survey. The resultant area of the bright survey, after discarding the underexposed edges, is 180.8 arcmin$^2$ and the FWHM of the point-spread function (PSF) is 1.″5. The mosaicked image is shown in Figure 1 (Plate 5). The images formed by median combining sequential blocks of 100 registered exposures in the faint survey were average combined to construct the image of the faint survey area. After discarding the underexposed edges, the resultant area of the faint survey is 2.21 arcmin$^2$ and the FWHM of the PSF is 1.″4. The image is shown in Figure 2 (Plate 6).

The time and spatial variation of the background in the raw $K'$-band exposures do not represent simply the variation in detector sensitivity but include contributions from scattered light, emission from dust particles on the optical surfaces, and ambient thermal emission from the telescope structure. In order to minimize the influence of the time variation of the background, a sky image was subtracted from each exposure. For the faint survey, the sky images were constructed from the median combination of blocks of 100 exposures and subtracted from each of the 100 exposures making up the block. For the bright survey, the sky images were constructed from the median combination of exposures taken at the four preceding and four following grid positions in the same scan. In the final iteration, detected objects were masked and the area they covered was ignored in constructing the median combination.

Variations in detector sensitivity were corrected by dividing with a flat-field image after subtracting a sky image from each exposure. The flat-field image was constructed from a combination of a dome flat and an illumination correction. A dome flat was obtained for each night by differencing observations of a white screen with the calibration lamp on and off. The dome flat is free of contamination from ambient thermal emission but suffers from uneven illumination. An illumination correction was constructed from sky images and dark exposures. The sky images were corrected for thermal stray light, which changed along the rows, by subtracting a quadratic function of row number. A dark exposure was made with a cold, opaque shutter in the filter wheel blocking all external radiation and was subtracted from a stray light corrected sky image to make a sky flat. The flat-field image was then obtained by multiplying the dome flat by a sky flat that had been divided by the dome flat and smoothed with a $32 \times 32$ pixel box median filter. A flat-field image was constructed for each row in each scan of the bright survey and for each block of 100 exposures in the faint survey. The effectiveness of the correction for variations in detector sensitivity was confirmed by comparing the flux of a standard star measured on a $6 \times 6$ grid of positions on the array.

The photometric standard stars were taken from the United Kingdom Infrared Telescope (UKIRT) faint standard stars (Casali & Hawarden 1992) and the Infrared Imaging Spectrograph (IRIS) faint standard stars referred to the Carter system (Carter & Meadows 1995). The transformation between these two systems is

$$K_{\rm Carter} - K_{\rm UKIRT} = 0.01 - 0.017(J-K) \quad (1)$$

(Leggett, Smith, & Oswalt 1993). The colors of observed standard stars were $0 \lesssim (J-K) \lesssim 0.9$; thus, the difference of the two systems is less than 0.01 mag and negligible. Several

[5] IRAF is distributed by the NOAO, which is operated by the Association of Universities for Research in Astronomy, Inc., under cooperative agreement with the NSF.

[6] STSDAS is distributed by the STScI, which is operated by the Association of Universities for Research in Astronomy, Inc., for NASA.

standard stars were observed at every night, and the accuracy of the air-mass correction was $\sigma_K \approx 0.02$ mag. Similarly to McLeod et al. (1995), we detected no color term between the $K'$ filter and the $K$ filter from the observation of the standard stars. We thus estimate the color term simply using the filter isophotal wavelengths from Tokunaga (1997) (originally from Cohen et al. 1992 for the $H$ and $K$ filter), and derived the relation

$$\Delta_K \equiv K' - K = 0.04(H-K) . \quad (2)$$

Since $H-K = 0.2 \sim 0.3$ is typical for nearby galaxies (Gavazzi & Trinchieri 1989) and $0 \lesssim H-K \lesssim 0.8$ is expected for galaxies in the bright survey at $z \lesssim 1$ (Eisenhardt & Lebofsky 1987), the magnitude difference between $K'$ and $K$ was estimated as $\Delta_K \lesssim 0.03$. The number count error $\Delta_n$ propagated from $\Delta_K$ is given by

$$\frac{\Delta_n}{n} = 2.3\alpha\Delta_K , \quad (3)$$

where $\alpha \equiv d \log n/dm_K$ is the slope of galaxy counts. Even if we consider an extremely steep slope of $\alpha = 0.67$ at $K < 16$ from Gardner et al. (1993), the difference $\Delta_K \lesssim 0.03$ mag yields a negligible count error of $\Delta_n/n \lesssim 0.05$. Therefore, we will not distinguish between $K'$ and $K$ in the remainder of this paper.

## 4. ANALYSIS

### 4.1. *Detection and Photometry*

The Faint Object Classification and Analysis System (FOCAS; Valdes 1982; Jarvis & Tyson 1981) was used for the detection and the photometry of objects. It convolves an image by a user specified filter, then collects adjacent pixels that are above a user specified threshold from the sky background that is determined simultaneously, and decides that a set of connected pixels, if more than a user specified number of pixels, is an object. These three detection parameters—the convolution filter, the surface brightness threshold, and the minimum area—were adjusted to maximize the completeness while minimizing false detections by simulations. We prepared artificial field images with a Gaussian random noise field and stellar profiles, then tried to detect the artificial objects and measure their magnitudes using various sets of detection parameters. A $\sigma = 1$ pixel Gaussian of $5 \times 5$ pixels was used for the convolution filter, and the area of 5 connected pixels was adopted for the minimum area of object. The corresponding surface brightness threshold was $\mu_K = 21.3$ mag arcsec$^{-2}$ for the bright survey and $\mu_K = 23.3$ mag arcsec$^{-2}$ for the faint survey.

FOCAS measures four flux parameters such as core, aperture, isophotal, and "total" magnitudes. We chose the FOCAS "total" magnitude, which measures the flux within a region obtained by expanding the detection isophote by a factor of 2, because it is more stable than other flux parameters. This is because the photometric corrections of the aperture magnitude become large for nearby bright galaxies, and the apertures of the isophotal magnitude for faint objects are so small that the large fraction of flux is lost with the adopted parameters.

We carried out many simulations to examine the completeness and the photometry. We added a small number of artificial objects to the resultant mosaicked images in order not to change the number density of objects, then detected the objects and measured their magnitudes with the same FOCAS parameters, and compared their FOCAS "total" magnitudes with the input magnitudes if they were recovered. We repeated this until enough objects were examined.

For the bright survey, both simulated stellar profiles and galaxy profiles were considered in the simulations. The model PSF was used to construct the simulated stellar profiles and was also used to construct the simulated galaxy profiles by convolving the profiles of the model galaxy with it. The model PSF was constructed by fitting a Moffat function to the radial profile of the observational PSF, which was generated by the average of about 20 bright stars in the resultant mosaicked image. The model galaxies of different apparent magnitudes were generated by placing a galaxy with some absolute magnitude at different redshifts. To be consistent with the redshift survey of Songaila et al. (1994), which presented $z_{\rm median} = 0.579 \pm 0.1$ at $18 < K < 19$, the absolute magnitude $M_K = -23.75$ mag at $z = 0$ was determined for a model galaxy, which should give an apparent magnitude of $K = 18.5$ at $z = 0.6$. We adopted $(h, \Omega_0, \lambda_0) = (0.6, 0.2, 0.0)$, where $h = H_0/100$ km s$^{-1}$ Mpc$^{-1}$, while other choices of the cosmological parameters have only small difference at redshifts concerned ($z < 1$). The $K$-correction was derived by linearly interpolating and extrapolating the typical near-infrared colors of nearby galaxies, $H-K = 0.25$ and $J-K = 0.95$ (Gavazzi & Trinchieri 1989), thus leading to $-0.56$ mag at $z = 0.32$ and $-0.67$ mag at $z = 0.79$. No evolutionary correction was applied. An exponential disk profile was adopted for the radial distribution of surface brightness of the model galaxies. The internal extinction was neglected and the inclination was set randomly. The central surface brightness at $z = 0$ was adopted as $\mu_K(0) = 17.5$ mag arcsec$^{-2}$ (Giovanelli et al. 1995; data originally from Peletier et al. 1994; de Jong & van der Kruit 1994) with an uniform dispersion of $\pm 0.4$ mag. The half-light radius of the $K = 19$ model galaxy was $0''.75$ and comparable to the PSF.

For the faint survey, only simulated stellar profiles that were constructed from the model PSF were considered in the simulations, because galaxies become smaller at fainter magnitude, and, furthermore, the Poisson errors of galaxy counts of the faint survey were so large that the difference of estimated completeness for detecting either stars or galaxies would be negligible. The model PSF was constructed by fitting a Moffat function to the radial profile of the observational PSF, which was generated by the average of two bright stars in the resultant mosaicked image.

Five artificial objects consisting of either stellar profiles or galaxy profiles were added to the resultant image of the bright survey for each run of the simulation, and we carried out a total of 1760 runs for the stellar profiles and 2000 runs for the galaxy profiles at $15.0 \le K \le 20.5$. Only one artificial object was added to the resultant image of the faint survey for each run, and we carried out a total of 5000 runs at $18.0 \le K \le 22.8$. The results of these simulations are presented in Figure 3. The limiting magnitude with 80% completeness of the bright survey was $K = 18.8$ for simulated galaxy profiles and $K = 19.1$ for simulated stellar profiles. This limiting magnitude was $K = 21.2$ for the faint survey.

The number of false detections due to noise was estimated by detecting "negative" objects. The signs of the resultant images were reversed, and then the procedure of detection and photometry was repeated with the same FOCAS parameters except for the detection threshold below the sky, which was adjusted so that the average of the

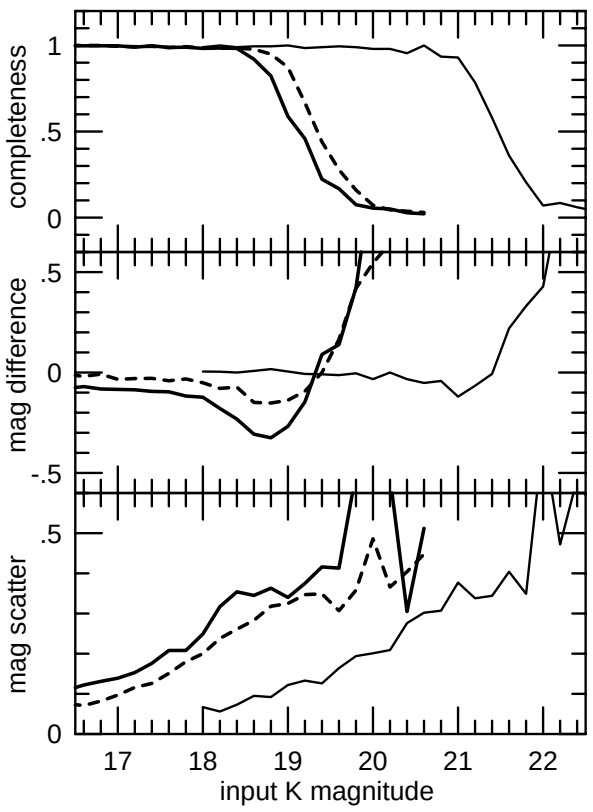


FIG. 3.—Completeness and photometry estimated from the simulations of detecting artificial objects added to the resultant mosaicked images of the bright and faint surveys. The detection rate or the completeness (*top panel*), the average of magnitude difference between the input magnitude minus the FOCAS "total" magnitude of detected objects (*middle panel*), and the magnitude scatter or the rms of magnitude differences (*bottom panel*) are shown as a function of the input magnitude of objects. The dashed and solid lines show the results for the bright survey for artificial stellar profiles and artificial galaxy profiles, respectively. The thin solid line shows the result for the faint survey with the only use of artificial stellar profiles.

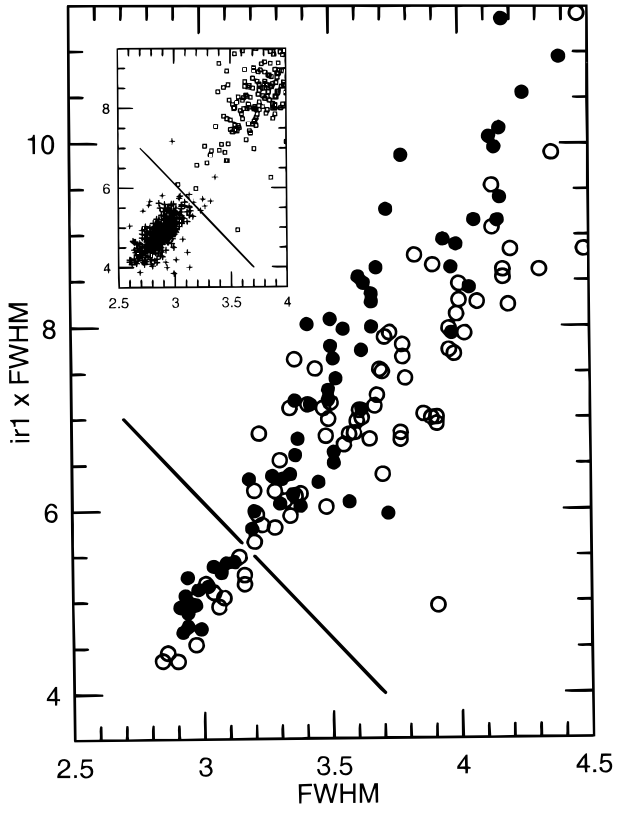


FIG. 4.—FWHM vs. ir1 × FWHM diagram used to separate stars and galaxies in the bright survey. FWHM and ir1 are in the pixel units, and the FWHM of PSF was about 3.0 pixels. The filled circles represent the objects of $16 < K < 17$, and the open circles for those of $17 < K < 17.5$. The objects at the lower left-hand side of the boundary (*thick line*) are compact and classified as stars, while the objects at the upper right-hand side of the boundary extending to outside this figure are diffuse and classified as galaxies. The inset shows the plots for the simulated stellar profiles and galaxy profiles of $17 < K < 17.5$ that were used for the completeness and photometry simulations in the bright survey. The pluses represent the simulated stellar profiles and the open squares represent the simulated galaxy profiles. The simulated stellar profiles are well confined in the lower left-hand side of the boundary.

global sky for detection was consistent with that for the "positive" detection. The estimated false detections in the bright survey were very few at the FOCAS "total" magnitude of $K < 19$, but they started to contribute toward fainter magnitudes. Only a few false detections were estimated in the faint survey.

### 4.2. *Star-Galaxy Separation and Star Counts*

Stars and galaxies in the bright survey were separated based on two morphological parameters, the FWHM and the ir1, where the FWHM was measured by Gaussian fitting of the radial profile by IRAF task IMEXAMINE and the ir1 was the intensity-weighted first-moment radius that was measured by FOCAS. The bright objects at $K < 16$ were easily separated based on the FWHM only. The objects at $16 < K < 17.5$ were separated on the FWHM–ir1 × FWHM diagram as shown in Figure 4. Because no clear separation was found for fainter objects, we did not attempt to separate stars and galaxies at $K > 17.5$. In the inset in this figure, we also plot the simulated stellar and galaxy profiles at $17.0 < K < 17.5$, which were used for the completeness and photometry simulations. It clearly shows that simulated stellar profiles are well confined in the lower left-hand side of the boundary and separated from simulated galaxy profiles. No simulated galaxy profiles was misclassified as stars, and only a few simulated stellar profiles were misclassified as galaxies. The distribution in the diagram of simulated stellar profiles seems to be slightly different from that of observed stars; however, the rate of misclassification from stars to galaxies was estimated as only $\lesssim 4\%$ and negligible compared with the Poisson errors of star counts and galaxy counts, even if the boundary was shifted 0.1 pixel smaller in the FWHM. The distribution in the diagram of simulated galaxy profiles seemed to be somewhat different from that of observed galaxies. However, the simulated galaxy profiles modeled a typical galaxy and the overall distribution of their morphological parameters was similar to that of the observed galaxies. The difference in distribution contributed by compact galaxies would just become impressive when the boundary region for the star-galaxy separation was closed up. Because we found the separation in the plots of the observed objects at $K < 17.5$, and because the estimated rate of misclassification from stars to galaxies were negligible, we did not make any corrections for misclassification of the star-galaxy separation. The $K$-band star counts to $K = 17.25$ obtained from the bright survey are tabulated in Table 1. Since the brightest star ($K \lesssim 11.7$) in the field center of the bright survey was

TABLE 1

THE K-BAND STAR COUNT

| K | Raw $N^a$ | Completeness[b] | $n^c$ | Error[c] |
|---|---|---|---|---|
| 12.0–12.5..... | 1 | 0.998 | 39.9 | 39.9 |
| 12.5–13.0..... | 1 | 0.998 | 39.9 | 39.9 |
| 13.0–13.5..... | 7 | 0.998 | 279 | 106 |
| 13.5–14.0..... | 6 | 0.998 | 240 | 97.8 |
| 14.0–14.5..... | 3 | 0.998 | 120 | 69.1 |
| 14.5–15.0..... | 5 | 0.998 | 200 | 89.3 |
| 15.0–15.5..... | 11 | 0.998 | 439 | 132 |
| 15.5–16.0..... | 6 | 0.998 | 240 | 97.8 |
| 16.0–16.5..... | 6 | 0.998 | 240 | 97.8 |
| 16.5–17.0..... | 10 | 0.998 | 399 | 126 |
| 17.0–17.5..... | 11 | 0.995 | 440 | 133 |

[a] Raw counts of detected stars in the specified magnitude range.

[b] The average of completeness for $15 \leq K \leq 17$ was presented at $K \leq 17$.

[c] Corrected star counts and the errors per magnitude per square degree.

used as a guide for the center, it was not used for the later analysis. In the faint survey, we did not attempt to separate stars and galaxies except for the two obvious bright stars.

In order to estimate the star counts at $K > 17.5$ and their contribution to the total counts, the SKY version 4 (Cohen 1994, 1995), which is a refinement of the Galaxy model for the infrared point source sky originally developed by Wainscoat et al. (1992), was fitted to the star counts at $K < 17.5$. Two parameters of the model, the solar displacement $z_\odot$ and the halo-to-disk ratio, were determined as $z_\odot = 16.5 \pm 2.5$ pc and halo:disk $= 0.56 \pm 0.03$ times that of the SKY version 1 (Wainscoat et al. 1992) by the same procedure as that used by Cohen (1995). Both values were consistent with those determined by Cohen (1995), 15.5 pc and about 0.45 times the SKY version 1, based on far-ultraviolet and mid-infrared source counts. The details will be described in another paper.

The star counts and the fitted model are plotted in Figure 5. By extrapolating the fitted model to $K > 17.5$, the contributions of the star counts to the total counts were estimated as about 7% at $K = 18$, and 5% at $K = 19$, which were comparable to the Poisson errors of galaxy counts of the bright survey. Therefore, we subtracted the predicted star counts from the total counts to derive the galaxy counts at

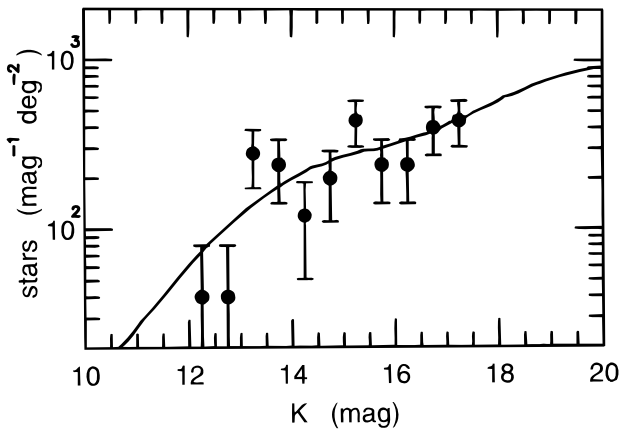


FIG. 5.—K-band star counts per magnitude per square degree in the SGP region. The filled circles represent the data obtained from the bright survey, and the solid line represents the fitted model of the SKY version 4 (Cohen 1995).

$K > 17.5$ for the bright survey. Compared to the Poisson errors of galaxy counts of the faint survey, the contributions of star counts were negligible; therefore, we did not subtract the predicted star counts for the faint survey.

## 5. GALAXY COUNTS

The galaxy counts at $K < 18$ from the bright survey were derived as follows: The FOCAS "total" magnitudes of objects were corrected to total magnitudes based on the simulations, and the number of galaxies in a specific magnitude range was counted, then the small incompleteness was corrected based on the simulations. The galaxies at $17.5 < K < 18.0$ were not separated from stars; therefore, their number was estimated by subtracting the predicted star counts from the total counts.

This standard procedure became unsatisfactory at faint-end magnitudes of the bright survey, because systematic biases existed close to detection limit. Because the scatter of error in photometry increases rapidly toward fainter magnitudes, and because fainter galaxies are more numerous than brighter galaxies, more faint galaxies are counted in the brighter magnitude bin than bright galaxies are counted in the fainter magnitude bin, then the number counts are altered. Furthermore, faint objects are preferentially brightened by noise to come into detection.

In order to avoid the problem, the galaxy counts at $K = 18.25, 18.75, 19.25$ from the bright survey were derived as follows (a similar attempt was made by Smail et al. 1995 in optical counts): We first generated the transfer matrix, $T_{ij}$, each element of which gives the fraction of galaxies with a total magnitude, $m_{\rm total} = m_j$, that was detected at the FOCAS "total" magnitude, $m_{\rm FOCAS} = m_i$, based on the simulations. We then generated the probability matrix, $P_{ji}$, each element of which gives the probability that a galaxy detected at the FOCAS "total" magnitude, $m_{\rm FOCAS} = m_i$, is a galaxy with the total magnitude, $m_{\rm total} = m_j$, as

$$P_{ji} = T_{ij} n_j / \sum_k T_{ik} n_k \,, \tag{4}$$

where $n_j$ is the number of galaxies at the total magnitude, $m_{\rm total} = m_j$. The number of stars at a specific FOCAS "total" magnitude, $N_i^s = N^{\rm star}(m_{\rm FOCAS} = m_i)$, was estimated by multiplying the number of stars at the total magnitude predicted by the star count model, $N_j^s = N^{\rm star}(m_{\rm total} = m_j)$, by the transfer matrix for stellar profiles, $T_{ij}^s$, and summing over total magnitudes as

$$N_i^s = \sum_j T_{ij}^s N_j^s \,. \tag{5}$$

The number of galaxies at a specific FOCAS "total" magnitude, $N_i^g = N^{\rm galaxy}(m_{\rm FOCAS} = m_i)$, was estimated by subtracting the estimated number of stars, $N_i^s$, and the number of false detections, $N_i^f$, from the total number of objects, $N_i^t$, at the specific FOCAS "total" magnitude, yielding $N_i^g = N_i^t - N_i^s - N_i^f$. Then the number of detected galaxies with a specific total magnitude, $N_j^g = N^{\rm galaxy}(m_{\rm total} = m_j)$, was estimated by multiplying the number of galaxies at the FOCAS "total" magnitude, $N_i^g$, by the probability matrix for galaxy profiles, $P_{ji}^g$, and summing over FOCAS "total" magnitudes as

$$N_j^g = \sum_i P_{ji}^g N_i^g \,. \tag{6}$$

We corrected $N_j^g$ for the incompleteness and finally derived the galaxy count.

The slope index of galaxy counts, $\alpha$, was presumed for the calculation of the probability matrix, $P_{ji}$, as $\alpha_1 = 0.67$ at $K < 16$, $\alpha_2 = 0.49$ at $16 < K < 18$, and the slope index $\alpha_3$ at $K > 18$ was left as a free parameter, because the matrix $P_{ji}$ at the magnitude concerned was dependent almost only on $\alpha_3$ and independent of $\alpha_1$ and $\alpha_2$. The parameter $\alpha_3$ was then adjusted to a value of $\alpha_3 = 0.28$ to be consistent with the derived slope for which $\alpha = 0.276$ from $K = 18.25$ to 18.75 or $\alpha = 0.277$ from $K = 18.25$ to 19.25. By this procedure, the slope index $\alpha_3$, and therefore the galaxy counts, was well determined. For example, an assumed slope of $\alpha_3 = 0.40$ leads to the derived slope for which $\alpha = 0.29$ from $K = 18.25$ to 18.75 or $\alpha = 0.32$ from $K = 18.25$ to 19.25. A slope of $\alpha = 0.28$ agrees well with $\alpha = 0.26$ at $K > 18$ found by Gardner et al. (1993).

Following the standard procedures, the galaxy counts at $K < 20$ from the faint survey were corrected for incompleteness and magnitude difference arising from photometry errors, and the galaxy counts at $20 < K < 22$ were derived using the probability matrix, $P_{ji}$. We assumed $\alpha_3 = 0.26$ at $K > 18$ (Gardner et al. 1993) for the estimation of the $P_{ji}$, because the Poisson errors of the galaxy counts at $K > 20$ were too large to determine a more precise slope of $\alpha_3$. Since the predicted contribution of star counts was negligible compared with the Poisson error of the galaxy counts, the total number of objects except for the two stars was used as the number of galaxies.

## 6. RESULTS

The $K$-band galaxy counts we obtained are tabulated in Table 2. The raw counts of galaxies of the bright survey at $K > 16.5$ and those of the faint survey at $K > 20.0$ are not integers because the predicted star counts were subtracted and the probability matrix, $P_{ji}$, was used. The errors given for the counts include only the Poisson errors defined as a square root of the raw number of objects and false detections. The $K$-band galaxy counts at $16 < K < 22$ are plotted in Figure 6, to be compared with other observations. It should be noted that the faintest points of each surveys are unreliable because their completenesses is small, $\lesssim 50\%$, and large corrections were needed.

TABLE 2

THE $K$-BAND GALAXY COUNT

| $K$ | Raw $N$[a] | Completeness[b] | $n$[c] | Error[c] |
|---|---|---|---|---|
| The Bright Survey | | | | |
| 12.5–13.5..... | 1 | 0.998 | 20.0 | 20.0 |
| 13.5–14.5..... | 2 | 0.998 | 39.9 | 28.2 |
| 14.5–15.5..... | 8 | 0.998 | 160 | 56.5 |
| 15.5–16.5..... | 33 | 0.998 | 659 | 115 |
| 16.5–17.5..... | 114 | 0.996 | 2290 | 214 |
| 17.5–18.0..... | 143 | 0.989 | 5740 | 481 |
| 18.0–18.5..... | 246 | 0.982 | 9980 | 682 |
| 18.5–19.0..... | 283 | 0.821 | 13700 | 1070 |
| 19.0–19.5..... | 178 | 0.375 | 18900 | 2270 |
| The Faint Survey | | | | |
| 18.0–19.0..... | 2 | 0.994 | 3280 | 2320 |
| 19.0–20.0..... | 8 | 0.991 | 13200 | 4650 |
| 20.0–21.0..... | 13.8 | 0.964 | 23400 | 6350 |
| 21.0–22.0..... | 10.5 | 0.527 | 32500 | 15800 |

[a] Raw counts of detected galaxies in the specified magnitude range.

[b] The average of completeness for $15 \leq K \leq 17$ was presented at $K \leq 17$.

[c] Corrected galaxy counts and the errors per magnitude per square degree.

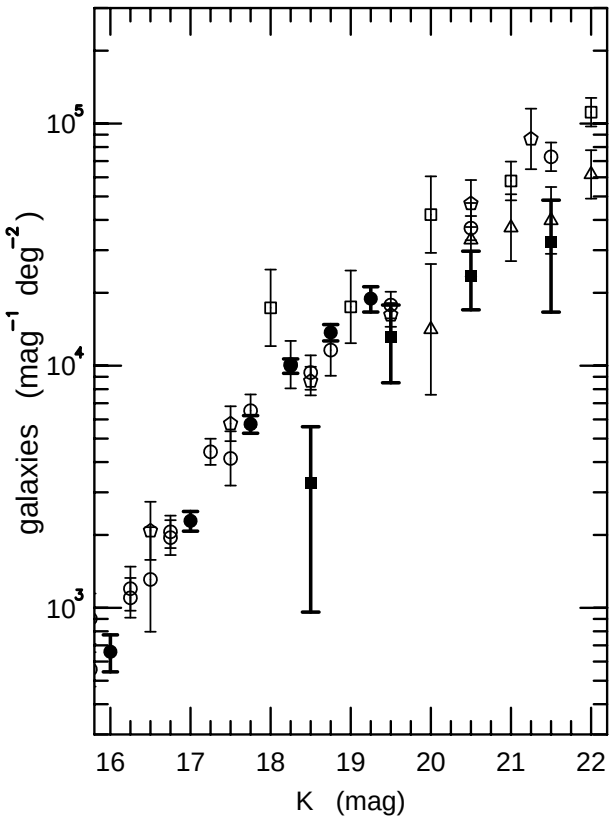


FIG. 6.—$K$-band galaxy counts per magnitude per square degree. The filled circles represent the data obtained from the bright survey, and the filled squares represent those from the faint survey. We note that the faintest points of each survey become unreliable because their completenesses were so small, $\lesssim 50\%$, and the large corrections were needed. The open circles represent the data of the Hawaii Medium Wide Survey, Hawaii Medium Deep Survey, and Hawaii Deep Survey compiled by Gardner et al. (1993) and Cowie et al. (1994), the open pentagons represent data from McLeod et al. (1995), the open triangles represent data from Djorgovski et al. (1995), and the open boxes represent data from Moustakas et al. (1997).

We estimated the field to field variations of galaxy counts due to clustering from angular correlation functions. For an angular correlation function of the power-law form $w(\theta) = A_w\theta^{-\gamma}$ and a circular top-hat window function of angular radius of $\theta_0$, the rms variation due to clustering is

$$\sigma_w = f(\gamma)w(\theta_0)^{1/2}\bar{N}\ , \qquad (7)$$

where $f(\gamma) \sim 1$ and $\bar{N}$ is the mean number of galaxies. From Lidman & Peterson (1996) the angular correlation was $\log_{10} w(\theta_0) \approx -2.5$ for $21 < I < 22$ and $\theta_0 = 7''.6$, each of which corresponds to $18 < K < 19$, where $I-K \sim 3$ (Gardner 1995b) and to the area of the bright survey. Then the rms variation due to clustering of the bright survey at its faintest magnitudes was estimated as $\sigma_w \sim 0.056\bar{N}$, which was comparable to the Poisson errors. The variation due to clustering of the faint survey was estimated from the angular correlation of $w(\theta) = (\theta/1''.4)^{-0.8}$ for $K \leq 21.5$ measured by Carlberg et al. (1997) from the survey area of 27 arcmin$^2$. The angular radius corresponding to the area of the faint survey is $\theta_0 = 50''$, and its rms variation due to clustering was estimated as $\sigma_w \sim 0.24\bar{N}$, or 0.09 dex. Thus, the galaxy counts of the faint survey could be significantly affected by clustering.

The $K$-band galaxy counts obtained from the bright survey are most precise at $17.5 < K < 19.0$ because of its large survey area and agree well with other observations. These counts are therefore important to model deeper galaxy counts at $K > 20$ in small survey areas to constrain the geometry of the universe. In addition, we confirm that the steep increase of the galaxy counts shows a turnover around $K \sim 18$, as Gardner et al. (1993) found that the slope changed from $\alpha = 0.67$ to $\alpha = 0.26$ at $K \approx 17$. This indicates that the galaxies around K = 17–18 have the largest contribution to the extragalactic background radiation in the $K$ band, because at this magnitude the slope of the integrated luminosity begins to converge.

The $K$-band galaxy counts obtained from the faint survey have large errors, and they are slightly lower than other observations and the bright survey as shown in Figure 6. However, the faint survey is subject to large Poisson errors and field-to-field variations due to clustering as described before because of its small survey area. In addition, we can see in Figure 1 that objects are more sparsely distributed in the field of the faint survey than in the rest of the bright survey. Therefore, when these uncertainties are considered, the galaxy counts from the faint survey are still consistent with other observations.

In summary, we present new $K$-band galaxy number counts obtained from the $K'$-band surveys in the SGP region. The completeness and photometry corrections were estimated with simulations, and the galaxy counts were derived using the probability matrix, $P_{ji}$, at the faint-end magnitudes close to the detection limits in order to compensate for the photometry errors. The bright survey provides galaxy counts to $K = 18.75$, and they agree very well with other observations. The faint survey provides galaxy counts to $K = 20.5$, and they are slightly lower compared to other observations and to the bright survey. However, when all uncertainties are considered, they are still consistent with other observations. We also present the star counts toward the SGP at $K < 17.5$ obtained from the bright survey, which are important for studying the vertical structure of the Galaxy.

We acknowledge M. Cohen for fitting the SKY version 4 model to our star counts and the SSO staffs and K. Nakamura for their technical support for the observation. Y. Y. acknowledges the financial support from the Yamada Science Foundation for transport of the PICNIC camera and the Japanese IR team to Australia. T. M. was supported by the Grant-in-Aid for JSPS Fellows by the Ministry of Education, Science, and Culture, and this work has been supported in part by the Grant-in-Aid for Center of Excellence Research (07CE2002) of the Ministry of Education, Science, and Culture.

## REFERENCES

Carlberg, R. G., Cowie, L. L., Songaila, A., & Hu, E. M. 1997, ApJ, 484, 538
Carter, B. S., & Meadows, V. S. 1995, MNRAS, 276, 734
Casali, M., & Hawarden, T. 1992, JCMT-UKIRT Newsletter, No. 4, 33
Cohen, M. 1994, AJ, 107, 582
———. 1995, ApJ, 444, 874
Cohen, M., Walker, R. G., Barlow, M. J., & Deacon, J. R. 1992, AJ, 104, 1650
Cowie, L. L., Gardner, J. P., Hu, E. M., Songaila, A., Hodapp, K.-W., & Wainscoat, R. J. 1994, ApJ, 434, 114
de Jong, R. S., & van der Kruit, P. C. 1994, A&AS, 106, 451
Djorgovski, S., et al. 1995, ApJ, 438, L13
Eisenhardt, P. R., & Lebofsky, M. J. 1987, ApJ, 316, 70
Gardner, J. P. 1995a, ApJS, 98, 441
———. 1995b, ApJ, 452, 538
Gardner, J. P., Cowie, L. L., & Wainscoat, R. J. 1993, ApJ, 415, L9
Gardner, J. P., Sharples, R. M., Carrasco, B. E., & Frenk, C. S. 1996, MNRAS, 282, L1
Gavazzi, G., & Trinchieri, G. 1989, ApJ, 342, 718
Giovanelli, R., Haynes, M. P., Salzer, J. J., Wegner, G., Da Costa, L. N., & Freudling, W. 1995, AJ, 110, 1059
Glazebrook, K., Peacock, J. A., Collins, C. A., & Miller, L. 1994, MNRAS, 266, 65
Huang, J.-S., Cowie, L. L., Gardner, J. P., Hu, E. M., Songaila, A., & Wainscoat, R. J. 1997, ApJ, 476, 12
Jarvis, J. F., & Tyson, J. A. 1981, AJ, 86, 476
Kobayashi, Y., Fang, G., Minezaki, T., Waseda, K., & Nakamura, K. 1994, Proc. SPIE, 2198, 603
Leggett, S. K., Smith, J. A., & Oswalt, T. D. 1993, in IAU Colloq. 136, Stellar Photometry—Current Techniques and Future Developments, ed. C. J. Butler & I. Elliott (Cambridge: Cambridge Univ. Press), 66
Lidman, C. E., & Peterson, B. A. 1996, MNRAS, 279, 1357
McLeod, B. A., Bernstein, G. M., Rieke, M. J., Tollenstrup, E. V., & Fazio, G. G. 1995, ApJS, 96, 117
Moustakas, L. A., Davis, M., Graham, J. R., Silk, J., Peterson, B. A., & Yoshii, Y. 1997, ApJ, 475, 445
Peletier, R. F., Valentijn, E. A., Moorwood, A. F. M., & Freudling, W. 1994, A&AS, 108, 621
Smail, I., Hogg, D. W., Yan, L., & Cohen, J. G. 1995, ApJ, 449, L105
Songaila, A., Cowie, L. L., Hu, E. M., & Gardner, J. P. 1994, ApJS, 94, 461
Tokunaga, A. T. 1997, in Astrophysical Quantities, ed. A. Cox (4th ed.; New York: AIP), in press
Valdes, F. 1982, Faint Object Classification and Analysis System (Tucson: NOAO)
Wainscoat, R. J., Cohen, M., Volk, K., Walker, H. J., & Schwartz, D. E. 1992, ApJS, 83, 111
Yoshii, Y., & Peterson, B. A. 1995, ApJ, 444, 15
Yoshii, Y., & Takahara, F. 1988, ApJ, 326, 1

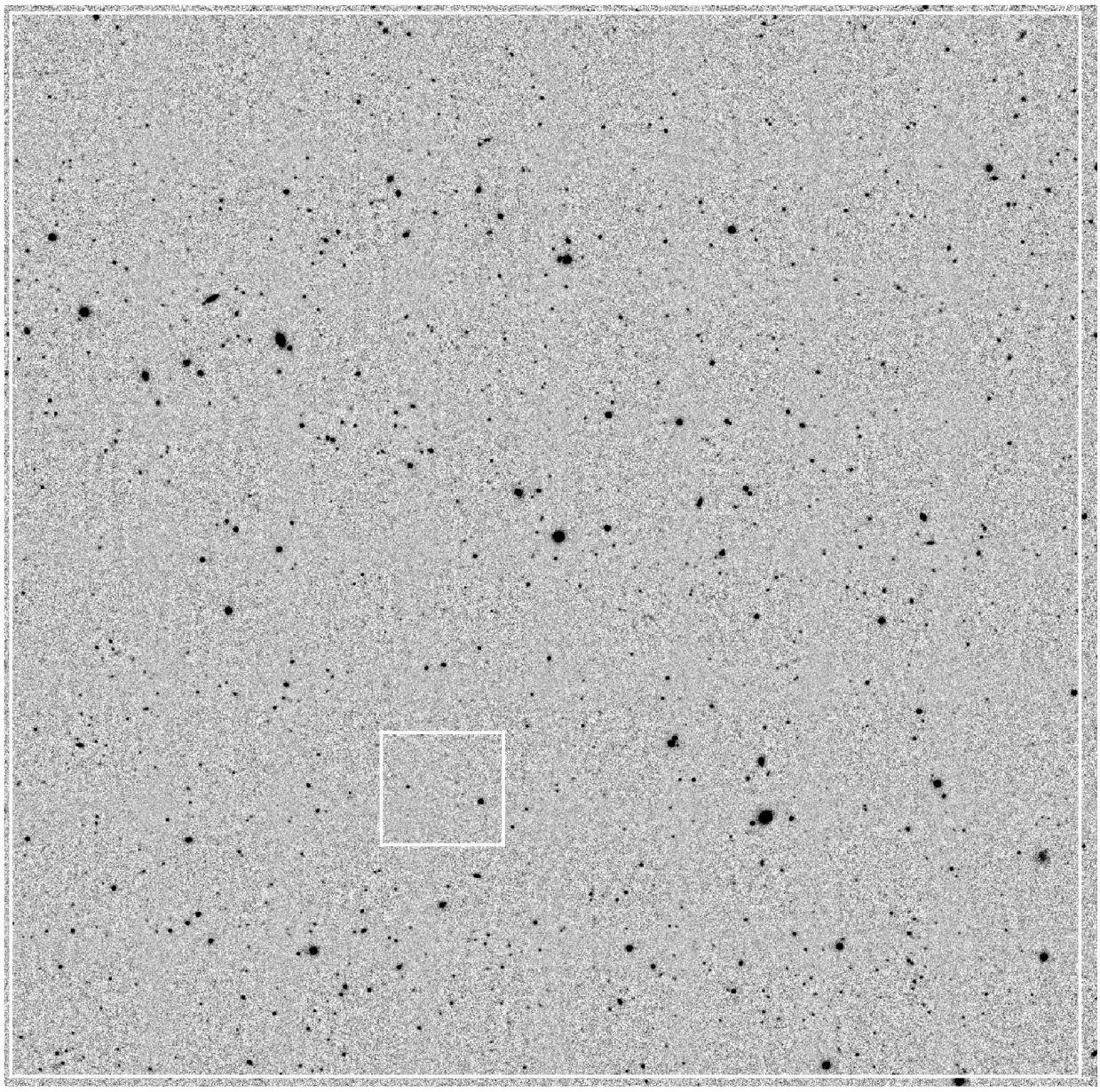

FIG. 1.—$K'$-band mosaicked image of the bright survey area in the SGP region. The large white box encloses the area of 180.8 arcmin$^2$ in which the galaxy counts were obtained. The small box at the lower left encloses the area of the faint survey. The overlapped regions between neighboring scan positions that have larger integration time can be seen as the areas of smaller noise background and make a checkered pattern.

MINEZAKI et al. (see 494, 112)

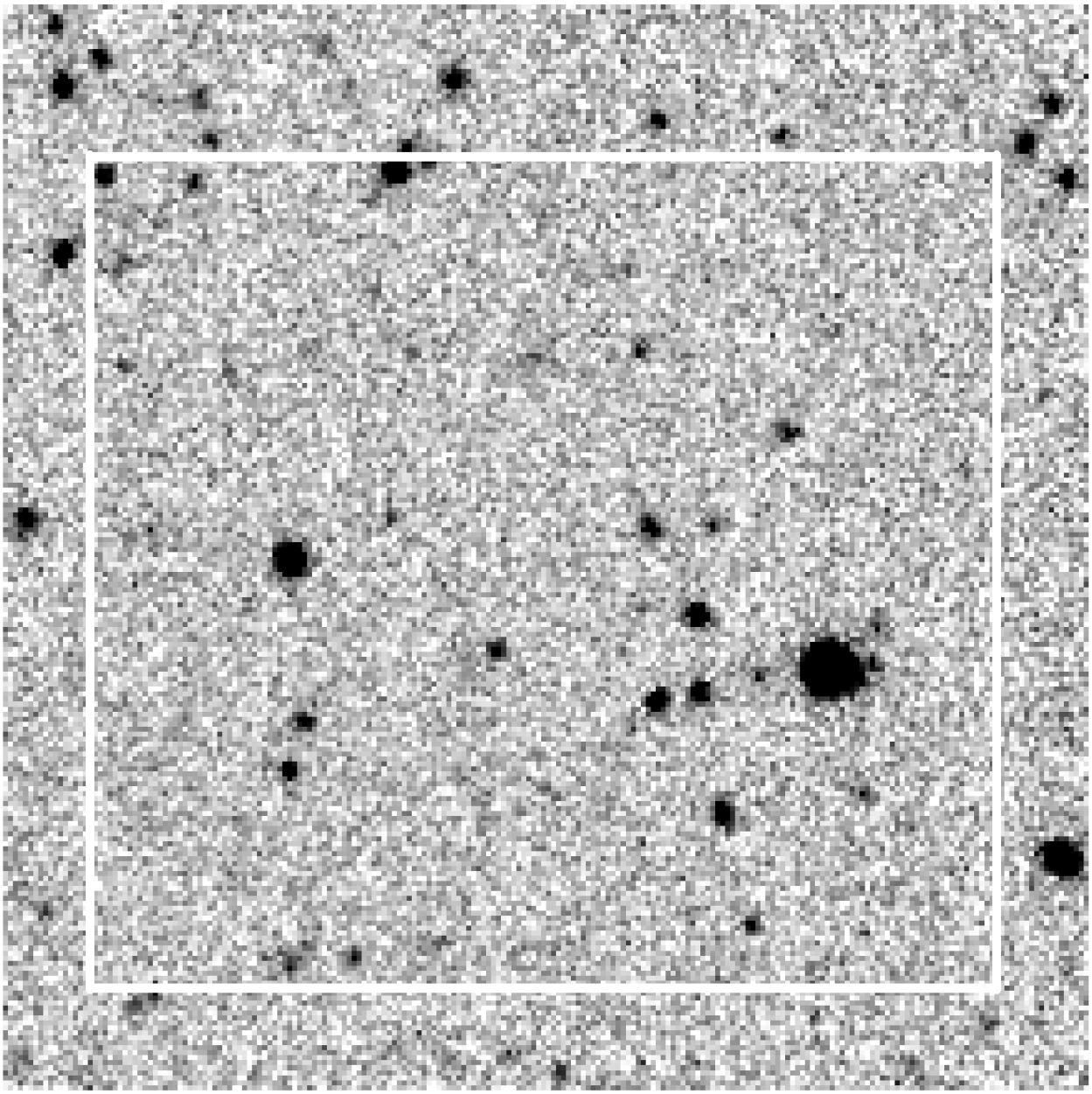

FIG. 2.—$K'$-band image of the faint survey area in the SGP region. The white box encloses the area of 2.21 arcmin$^2$ in which the galaxy counts were obtained. Two brightest objects seen in the area are stars.

MINEZAKI et al. (see 494, 112)

PLATE 6